arXiv:1604.06445v1 [cond-mat.mes-hall] 21 Apr 2016

Electronic and magnetic properties of single-layer MPX_3 metal phosphorous trichalcogenides

Bheema Lingam Chittari,[1,2] Youngju Park,[2] Dongkyu Lee,[2] Moonsup Han,[2] Allan H. MacDonald,[3] E. H. Hwang,[1,*] and Jeil Jung[2,†]

[1]*SKKU Advanced Institute of Nanotechnology, Sungkyunkwan University, Suwon, 16419, Korea*
[2]*Department of Physics, University of Seoul, Seoul 02504, Korea*
[3]*Department of Physics, The University of Texas at Austin, Austin, Texas 78712, USA*

We systematically investigate the electronic structure and magnetic properties of two dimensional (2D) MPX_3 (M= V, Cr, Mn, Fe, Co, Ni, Cu, Zn, and X = S, Se, Te) transition metal chacogenophosphates to examine their potential role as single-layer van der Waals materials that exhibit magnetic order. Our *ab initio* calculations predict that most of these single-layer materials are antiferromagnetic semiconductors. The band gaps of the antiferromagnetic states decrease as the atomic number of the chalcogen atom increases (from S to Se, Te), leading in some cases to half-metallic ferromagnetic states or to non-magnetic metallic states. We find that the phase transition from antiferromagnetic semiconductor to ferromagnetic half-metal can be controlled by gating or by strain engineering. The sensitive interdependence we find between magnetic, structural, and electronic properties establishes the potential of this 2D materials class for applications in spintronics.

PACS numbers: 75.70.Ak,85.75.Hh,77.80.B-,75.30.Kz,75.50.Pp

I. INTRODUCTION

Motivated by seminal studies which reported on the exfoliation of a single stable layer of graphene and presented transport measurements that revealed its Dirac fermion fingerprint,[1,2] research on ultrathin two dimensional (2D) materials has emerged during the last decade as one of the most active research topics in condensed matter physics. Two-dimensional materials are interesting in part because their properties can be modified *in situ* by adjusting gate voltages. Recently, interest has expanded beyond graphene to other layered van der Waals materials that offer alternative properties which are potentially useful for applications.[3] For example, one popular class of 2D materials is the transition metal dichalcogenides (TMDC)[4] which include semiconductors and metals, exhibit strong light-matter coupling,[5] and sometimes host ordered electronic states including charge density waves and superconductivity.[6–9] Magnetic order has, however, not yet been established in any two-dimensional material. Room-temperature magnetism in a single-layer material is an extremely attractive materials target because of the expectation that it would provide unprecedented electrical control of magnetic configurations and enable new classes of information processing devices that incorporate non-volatile memory elements more intimately.

Two dimensional magnetism is a very broad and fundamentally interesting topic in the theory of quantum matter.[10] One strategy to search for magnetism in isolated two-dimensional van der Waals materials is to explore the magnetic properties of single-layers exfoliated from a bulk material that exhibits robust magnetic order. Following this approach, recent theoretical studies have proposed a number of potentially magnetic single-layer van der Waals materials, including V based dichalcogenides[11], $FeBr_3$, chromium based $CrSiTe_3$ and $CrGeTe_3$ ternary tritellurides[12–17], CrX_3 trihalides[20,21], and $MnPX_3$ ternary chalcogenides[22,23]. The family of MPX_3 compounds, also known as transition metal phosphorous trichalcogenides, are known to exhibit magnetism for M=Mn and for a number of other metal atom species. The structures and magnetic properties of some bulk compounds have already been extensively studied.[24–44] Because of the van der Waals character of these materials, one focus of bulk materials research is to characterize ion intercalation properties.[45–49]

In this paper we present an *ab initio* study of the MPX_3 metal-phosphorous-trichalcogenide family of single-layer materials. We consider a broad range of 3d transition metals (M= V, Cr, Mn, Fe, Co, Ni, Cu, Zn) and chalcogen atoms (X = S, Se, Te) in an effort to explore the magnetic phases that can be expected as fully as possible. We explore how quasiparticle bands are modified when the magnetic configurations undergoes a transition from antiferromagnetic to ferromagnetic, or from magnetic to non-magnetic. Our results confirm the expected strong interdependence between magnetic configuration and structural properties, for example lattice constant or crystal symmetry, and explain a surprisingly strong dependence of exchange interaction strengths on electron density and strain.

The paper is structured in the following manner. We start in Sec. II by briefly summarizing specific details of our first principles electronic structure calculation details. In Sec. III we discuss our results for ground-state properties including structure, magnetic properties, and electronic band structure and density of states. Sec. IV is devoted to an analysis of the carrier-density dependence of the magnetic ground state, and to a study of the influence of strain on the magnetic phase diagram. Finally we close the paper in Sec.V with a summary and discussion of our results.

II. *AB INITIO* CALCULATION DETAILS

The study of the ground-state electronic structure and magnetic properties in this work has been carried out using plane-wave density functional theory as implemented in Quantum Espresso.[50] We have used the Rappe-Rabe-Kaxiras-Joannopoulos ultrasoft (RRKJUS) pseudoptentials for the semi-local Perdew-Burke-Ernzerhof (PBE) generalized gradi-

ent approximation (GGA)[51] together with the VdW-D2 correction[52]. We choose the GGA+D2 as a reference calculation because of the overall improvement of the GGA over the LDA[53] for covalent bond description, and add the longer ranged D2 correction to improve the description of binding between the layers. (The GGA typically performs poorly for van der Waals bonds.[54]) The magnetic solutions have also been compared with calculations employing the LDA+U scheme, using values for the onsite repulsion U that saturate the magnitude of the band gap in compounds that have semiconducting ground states. Comparisons were made with hybrid HSE functionals[55] to assess non-local exchange effects that could further influence the magnetic ground states. All structures were optimized without constraints until the forces on each atom reached 10^{-5} Ry/au. The self-consistency criteria for total energies has been set at 10^{-10} Ry and momentum space integrals were performed using a regularly spaced k-point sampling density of $16\times16\times1$,with a plane wave energy cutoff of 90 Ry. For the HSE calculation we used a coarser effective k-point sampling of $4\times4\times1$. The out-of-plane vertical size of the periodic supercell was chosen to be 25 $\AA$, which typically leaves an adequate vacuum spacing greater than 10 $\AA$ between two-dimensional layers.

III. STRUCTURAL AND MAGNETIC PROPERTIES

The atomic structure of MPX_3 transition metal chalcogenophosphate layers is anchored by $(P_2X_6)^{4-}$ bipyramids arranged in a triangular lattice which provide enclosures for transition metal atoms arranged in an hexagonal array. (See Fig. 1 for a schematic illustration of the single layer unit cell and the bulk atomic structure.) The bulk crystals consists of ABC-stacked single layer assemblies that are held together by van der Waals forces. Although the atomic structures of single layer transition metal phosphorous trichalcogenide crystals are similar to those of bulk crystals, small changes appear in response to the absence of the interlayer coupling, with distortions in the ground-state crystal geometries correlated mainly with the magnetic phase. The analysis of the magnetic properties is simplified by the fact that the magnetic moments develop almost entirely at the metal atom sites.

We calculate the magnetic ground-state and meta-stable magnetic configurations by identifying converged self-consistent ground states starting from different magnetic initial conditions that can be classified as either Néel antiferromagnetic (AFM), or ferromagnetic (FM), or nonmagnetic (NM) states when a triangular unit cell is used. The calculation indicates that most 2D MPX_3 crystals are semiconductors with localized magnetic moments that are ordered antiferromagnetically. We find that the use of chalcogen atoms with larger atomic numbers leads to an overall reduction of the energy band gap between valence and conduction bands. In the following we present an analysis of the structural and magnetic properties of representative 3d transition metal MPX_3 trichalcogenides, and discuss their underlying electronic bandstructures.

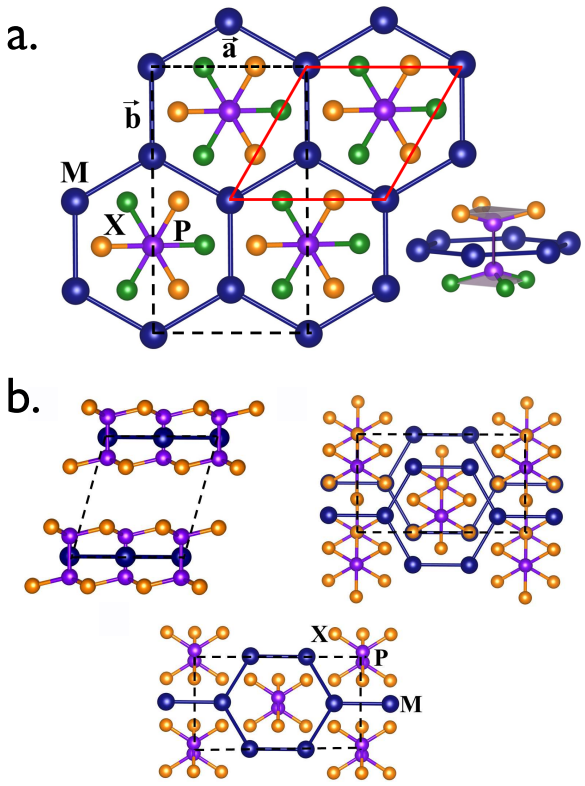

FIG. 1: (Color online) Schematic representation of the atomic structure of transition metal phosphorous trichalcogenide MPX_3 compounds in which $(P_2X_6)^{4-}$ bipyramids form a structural frame that can enclose different types of metal atoms. **a.** Atomic structure of a MPX_3 monolayer. A rectangular supercell is represented with black dashed lines while a smaller triangular lattice unit cell is represented by red solid lines. Each triangular unit cell contains two transition metal atoms (M) arranged in a honeycomb. Phosphorus (P) dimers are perpendicular to the plane at the center of each hexagon. Three sulfur atoms are bound to each of the P atoms, and the top and bottom trimers have a relative in-plane twist of 60° degrees. **b.** The lowest energy 3D-bulk structure consist of individual layers stacked in an ABC sequence. We present the structure from three viewpoints, a side view, a top in which the phosphorous atoms within a single layer lie on top of each other, and a view in which the transition metal atoms of two adjacent layers lie on top of each other.

A. Structural properties

The MPX_3 compounds that we study consist of V, Cr, Mn, Fe, Co, Ni, Cu, and Zn transition metal atoms with 3d valence electrons, combined with three different chalcogen atoms S, Se, and Te. We thus expand our study beyond the most common crystals in this class, the $MnPS_3$, $FePS_3$, $CoPS_3$, $NiPS_3$, $ZnPS_3$ thiophosphates whose bulk structure had been explored in past experiments.[24–40,46–49] We have optimized MPX_3 lattice structures using the unit cell shown in Fig. 1 for single layers and assuming ABC stacking for bulk. Given this framework, structures are characterized by the value of the in-plane lattice constant a, the (P-P) distance between the phos-

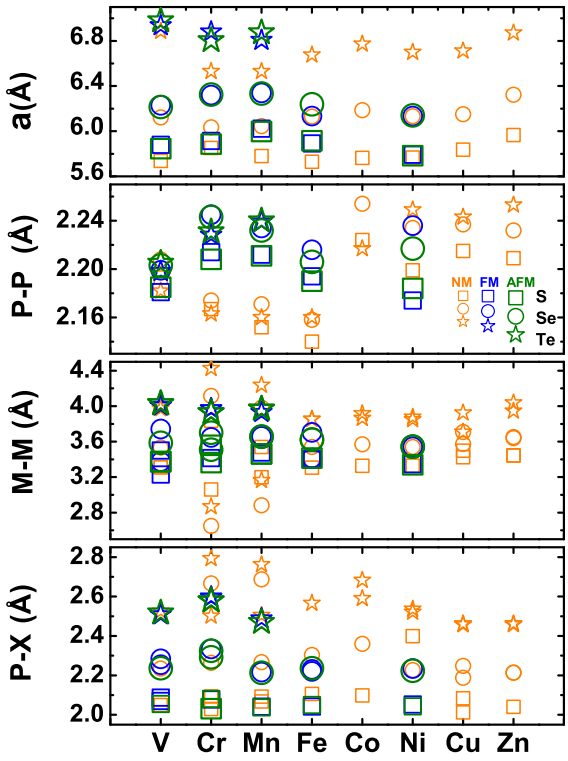

FIG. 2: (Color online) **a.** In-plane lattice constant, P-P bond length, M-M bond length and P-X bond length for different transition metal elements. Bond lengths increase with the size of the chalcogen atom (S- square, Se - circle, Te - star) but have a non-monotonic dependence on metal atom atomic number, and have a strong dependence on whether the magnetic state is NM (non-magnetic - organge), FM (ferromagnetic - blue), or antiferromagnetic (AFM-green).

phorous atoms, the (M-M) distance between metal atoms, and the (P-X) distance between metal and chalcogen atoms. The variation in the magnitude of these bond lengths as a function of the metal and chalcogen atom species, and magnetic configuration is illustrated in Fig. 2, and summarized numerically in Table I. Results are presented for all metastable magnetic states. The structures have a simple dependence on chalcogen atom size, with larger in-plane lattice constants and monolayer thicknesses (P-P distances) for larger chalcogens. However, the dependence of structure on metal atom atomic number is not straightforward. Experiments in the bulk MPS_3 observed a close correlation between the radius of the metal cation and the P-P distance of the thiophosphate bipyramid.[24] The non-monotonic variation of the metal cation radius with respect to atomic number is reflected in the P-P distance trend. However, our calculations show that bond lengths correlate more strongly with magnetic state than with metal atomic number.

P-P distances range between $2.15-2.3$ $\AA$ while M-M bond lengths vary by about 5% . The M-M bond lengths within an hexagon can be unequal, distorting the hexagonal lattice arrangement of the metal atoms as illustrated in Fig. S1 in the supplementary information. In general ferromagnetic states have the largest lattice constants, and antiferromagnets have intermediate lattice constants. The fact that the structural properties of these crystals are correlated with their magnetic configurations suggests the possibility of controlling magnetic properties by straining the lattice, as we will discuss more in detail in a later section.

The comparison between lattice parameters calculated within GGA and LDA with the experimental bulk structure that is summarized in Table II indicates important discrepancies between the GGA and LDA, and is consistent with the tendency of the LDA to overbind covalent bonds. The stronger LDA bonds leads to a global reduction of lattice constant and to a stronger distortion of the metal honeycombs. Within the LDA we find optimized lattice parameters that are (2-5%) shorter than in bulk experiments. The GGA agreement is good (0.5-1.6%) for $MnPS_3$, $FePS_3$, $CoPS_3$, $NiPS_3$ and $ZnPS_3$.

B. Magnetic properties

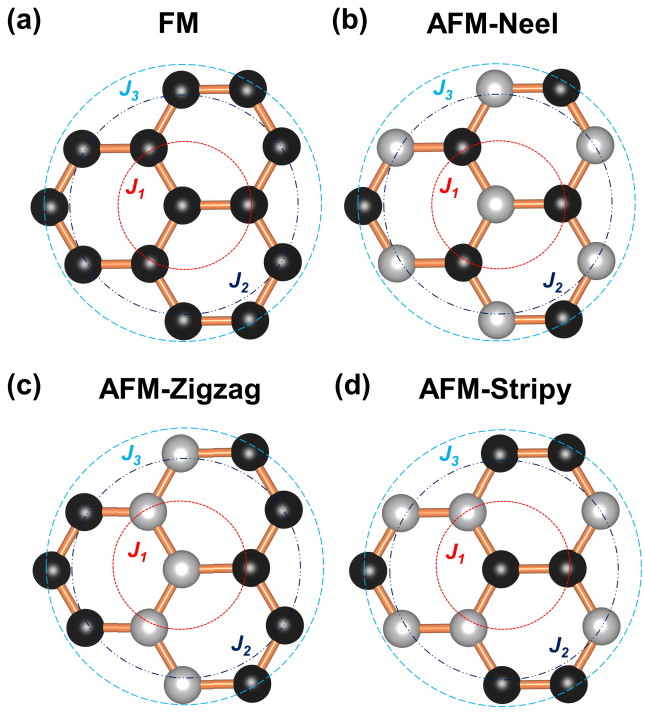

FIG. 3: (Color online) The top view of different magnetic ordering (a) ferromagnetic, (b) Néel, (c) zigzag and (d) stripy antiferromagnetic order between metal atoms in honeycomb lattice of MPX_3 compounds. The black and white spheres represent the up and down spins, respectively. The nearest neighbors are connected through different circles, the red color (dotted) circle connects the first nearest neighbors (NN), navy color (dashed and dotted) circle connects the next NN and blue (dashed) circle connects the next to next NN. J_1, J_2 and J_3, are the exchange interaction parameters between the metal atoms within each circles

TABLE I: Self-consistent theoretical M-M, P-P, and P-S bond lengths in $\AA$ for metastable magnetic states of single layer transition metal phosphorous trichalcogenide MPX_3 within GGA+D2. Double entries indicate bond length variations that distort the reference lattice structure.

MPX_3	X	M-M			P-P			P-X		
		NM	FM	AFM	NM	FM	AFM	NM	FM	AFM
VPX_3	S	3.313, 3.311	3.500, 3.230	3.377, 3.372	2.193	2.181	2.185	2.050	2.070, 2.087	2.055
	Se	3.535	3.743, 3.375	3.587	2.208	2.199	2.203	2.235	2.284, 2.254	2.236
	Te	3.976, 3.974	4.002, 4.005	4.030, 4.028	2.182	2.198	2.205	2.526	2.507	2.518
$CrPX_3$	S	3.060, 3.836	3.414	3.363, 3.558	2.167	2.214	2.208	2.093, 2.029	2.078	2.080, 2.031
	Se	4.115, 2.650	3.648	3.700, 3.510	2.174	2.245	2.243	2.264, 2.667	2.334	2.325, 2.292
	Te	4.426, 2.868	3.971,3.970	3.930, 3.928	2.163	2.228	2.231	2.501, 2.793	2.598, 2.596	2.578, 2.580
$MnPX_3$	S	3.199, 3.539	3.477	3.463, 3.462	2.152	2.212	2.211	2.092, 2.068	2.041	2.038
	Se	3.983, 2.883	3.660	3.657, 3.655	2.171	2.234	2.232	2.267, 2.687	2.217	2.213
	Te	4.236, 3.162	3.929	3.969, 3.967	2.160	2.239	2.240	2.505, 2.762	2.487	2.470
$FePX_3$	S	3.307	3.403, 3.397	3.463, 3.608	2.140	2.194	2.198	2.106	2.042	2.054, 2.047
	Se	3.540	3.705, 3.415	3.623, 3.624	2.158	2.216	2.206	2.304	2.220, 2.230	2.236
	Te	3.853, 3.855	-	-	2.16	-	-	2.566	-	-
$CoPX_3$	S	3.327	-	-	2.224	-	-	2.098	-	-
	Se	3.571	-	-	2.254	-	-	2.360	-	-
	Te	3.863, 3.916	-	-	2.217	-	-	2.590, 2.683	-	-
$NiPX_3$	S	3.329	3.344	3.339	2.199	2.174	2.184	2.399	2.052	2.043
	Se	3.540	3.541	3.544,3.543	2.234	2.236	2.217	2.227	2.235	2.224
	Te	3.848, 3.876	-	-	2.249	-	-	2.521, 2.536	-	-
$CuPX_3$	S	3.425, 3.499	-	-	2.215	-	-	2.012, 2.084	-	-
	Se	3.574, 3.708	-	-	2.237	-	-	2.188, 2.248	-	-
	Te	3.925, 3.709	-	-	2.243	-	-	2.457, 2.462	-	-
$ZnPX_3$	S	3.445, 3.443	-	-	2.209	-	-	2.040	-	-
	Se	3.652, 3.641	-	-	2.232	-	-	2.214, 2.213	-	-
	Te	3.946, 4.038	-	-	2.253	-	-	2.458, 2.462	-	-

Experimental study of magnetic properties of bulk Mn, Fe, Co, Ni thiophosphate sulphides have found antiferromagnetic ground states with Néel temperatures ranging between 82K$\sim$155K.[24] Here we find that magnetism persists in single layer MPX_3 compounds. The magnetic moments develop mainly at the localized metal atom sites, but the small spin polarization at the phosphorous and sulphur atoms is noticeable in the ferromagnetic configuration.

The late 3d transition elements Cr, Mn, Fe, Co and Ni stand out in the periodic table as elements that tend to order magnetically. The bonding arrangements of particular compounds can however enhance or suppress magnetism. in 2D MPX_3 crystals, the transition metal atoms hybridize relatively weakly with other transition metal atoms because they are contained within phosphorous trichalcogenide bipyramidal cages. The exchange interactions between the metal atoms are therefore mainly mediated by indirect exchange through the intermediate chalcogen and P atoms. Magnetic interactions can be examined by comparing ground state energies for different magnetic configurations. We compare antiferromagnetic, ferromagnetic and nonmagnetic state energies in V, Cr, Mn, Fe, Ni based compounds in Table III, where we find that the AFM phase is normally favored over the FM phase.

Because our calculations show that the magnetic moments are concentrated at the metal atoms sites we can characterizie the magnetic properties of the 2D MPX_3 by mapping the energy landscape to an effective honeycomb-lattice Heisenberg model:

$$H = \sum_{\langle ij \rangle} J_{ij} \vec{S}_i \cdot \vec{S}_j = \frac{1}{2} \sum_{i \neq j} J_{ij} \vec{S}_i \cdot \vec{S}_j \tag{1}$$

where $\vec{S}_i$ is the total spin magnetic moment of the atomic site i and J_{ij} is the exchange coupling parameters between two local spins. By evaluating the three independent energy differences between the four magnetic configurations[24,56,57] illustrated in Fig. 3, ferromagnetic (FM), Néel (AFM), zigzag AFM (zAFM), and stripe AFM (sAFM), and assuming that the magnetic interactions are short range, we can extract the nearest neighbor (J_1), next-nearest- (J_2), and next-next-nearest-neighbor (J_3) coupling constants:[57]

$$E_{\rm FM} - E_{\rm AFM} = 3(J_1 + J_3)\, \vec{S}_A \cdot \vec{S}_B \tag{2}$$

$$E_{\rm zAFM} - E_{\rm sAFM} = (J_1 - 3J_3)\, \vec{S}_A \cdot \vec{S}_B \tag{3}$$

$$E_{\rm FM} + E_{\rm AFM} - E_{\rm zAFM} - E_{\rm sAFM} = 8 J_2\, \vec{S}_A \cdot \vec{S}_A \tag{4}$$

where $\vec{S}_X$ is the average spin magnetic moment on the honeycomb sublattice X. The total energies of the zAFM and sAFM magnetic configurations, calculated using a rectangular unit cell geometry usually have higher energies than the average of the AFM solutions and FM solutions, implying that $J_2 > 0$. For the case of $FePS_3$, however, the zAFM has the lowest en-

TABLE II: Experimental and theoretical bulk lattice parameters in *Å* compared with two dimensional lattice parameters for transition metal phosphorous trichalcogenide MPX_3 within GGA+D2; a is the in-plane lattice constant and c′ is a layer thickness parameter, *i..e* it is the distance between the planes containing the three chalcogen atoms in a single MPX_3 layer. The values in parenthesis below the bulk c′(Å) values are the interlayer distances.

MPX_3	X	NM		FM		AFM	
		a(Å)	c′(Å)	a(Å)	c′(Å)	a(Å)	c′(Å)
	S	5.737	3.142	5.880	3.166	5.846	3.170
	S(bulk)	5.742	3.280	5.918	3.273	5.845	3.294
			(2.518)		(2.585)		(2.655)
	S(Expt)	-	-	-	-	-	-
VPX_3	Se	6.123	3.266	6.230	3.204	6.214	3.318
	Te	6.885	3.328	6.935	3.418	6.980	3.431
	S	5.851	3.071	5.914	3.032	5.885	3.336
	S(bulk)	5.862	3.116	5.913	3.185	5.934	3.301
			(2.624)		(2.506)		(2.465)
	S(Expt)	-	-	-	-	-	-
$CrPX_3$	Se	6.035	3.367	6.320	3.100	6.325	3.235
	Te	6.530	3.672	6.880	3.330	6.804	3.388
	S	5.780	2.952	6.023	3.256	5.997	3.246
	S(bulk)	5.787	2.875	6.018	3.125	5.993	3.268
			(2.456)		(2.567)		(2.562)
	S(Expt)	-	-	-	-	6.076	-
$MnPX_3$	Se	6.045	3.182	6.340	3.416	6.334	3.402
	Te	6.530	3.444	6.805	3.550	6.874	3.535
	S	5.730	2.808	5.891	3.150	5.958	3.180
	S(bulk)	5.736	2.969	5.874	3.313	5.921	3.217
			(2.386)		(2.840)		(4.368)
	S(Expt)	-	-	-	-	5.934	-
$FePX_3$	Se	6.130	2.911	6.134	3.347	6.239	3.214
	Te	6.676	3.038	-	-	-	-
	S	5.763	2.790	-	-	-	-
	S(bulk)	5.784	2.950	-	-	-	-
			(4.250)				
	S(Expt)	5.901	-	-	-	-	-
$CoPX_3$	Se	6.186	2.850	-	-	-	-
	Te	6.772	3.057	-	-	-	-
	S	5.766	2.974	5.792	3.064	5.783	3.042
	S(bulk)	5.763	2.995	5.789	3.062	5.779	3052
			(2.431)		(2.449)		(2.480)
	S(Expt)	-	-	-	-	5.813	-
$NiPX_3$	Se	6.132	3.086	6.134	3.100	6.140	3.142
	Te	6.700	3.208	-	-	-	-
	S	5.837	3.439	-	-	-	-
	S(bulk)	5.843	2.245	-	-	-	-
			(3.903)				
	S(Expt)	-	-	-	-	-	-
$CuPX_3$	Se	6.151	3.532	-	-	-	-
	Te	6.711	3.617	-	-	-	-
	S	5.966	3.230	-	-	-	-
	S(bulk)	5.973	2.564	-	-	-	-
			(3.025)				
	S(Expt)	5.971	-	-	-	-	-
$ZnPX_3$	Se	6.323	3.379	-	-	-	-
	Te	6.871	3.597	-	-	-	-

ergy. The average magnetic moment S at each lattice site obtained within the GGA+D2 are listed in Table IV.

Single-layer magnetic ordering temperatures T_c were estimated by running Monte Carlo simulations of the three-coupling-constant effective models using the Metropolis algorithm in lattice sizes up to N=16×32 with periodic boundary conditions,[58] and verified against calculations performed using Wang-Landau Monte Carlo sampling algorithm in smaller N=8×16 lattices.[59] We used the absolute magnetization per lattice $\langle|m|\rangle = \langle\left|\sum_i^N \vec{S}_i\right|\rangle/N$ as the order parameter to calculate both the Curie temperature for the ferromagnetic phase and the Neel temperature for the antiferromagnetic phase using the fact that $\langle|m|\rangle$ drops to zero in the former and acquires nonzero value in the latter for sufficiently large temperatures. We used the derivative maximum $d\langle|m|\rangle/d$T to estimate the critical temperatures. See the supplementary information for the plot of the representative results for the temperature dependent magnetization obtained in this way.

The calculated average values of the magnetic moments in the AFM configuration vary widely, e.g. assuming the values of 3.14, 4.16, 3.2, 0.8 and 1.14 μ_B for Cr, Mn, Fe, Co and Ni based sulphides, see Table IV. The magnitude of the magnetic moments have generally a relatively small change between 3%∼10% for most cases, except for the relatively large differences found for the ground states of $CoPS_3$ and $NiPSe_3$. We find that the magnetic moments in 2D MPX_3 develop almost entirely at the metal atom sites whereas in the bulk structure the phosphorous and chalcogens do acquire a small spin polarization that can be attributed to result from the interlayer coupling.

C. Band structure and density of states

Understanding the electronic properties of 2D MPX_3 layers is an essential stepping stone on the path toward possible integration in nanodevices. For spintronic applications of magnetic 2D materials, which seek to couple charge and spin degrees of freedom, it is desirable to understand how the electronic structure depends on the type of magnetic order. The spin resolved band structures of the lowest energy spin configuration, calculated within the GGA+D2 approximation, are presented in Fig. 4, and the associated densities-of-states are presented in Fig. 5. Single layer MPX_3 with M = V, Cr, Mn, Fe, Co, Ni, Cu, Zn transition metal atoms and X = S, Se, Te chalcogen atoms are considered. Band structures for some higher energy spin configurations are included in the supplementary material.

We find that AFMs are almost always gapped semiconductors, that the FM states are metallic, and that the NM phases can be either semiconducting or metallic. It follows that the MPX_3 class of materials includes almost all of the behaviors being studied in current spintronics research, including importantly both antiferromagnets and ferromagnets and both metals and insulators. The magnitude of the band gaps of the semiconducting 2D MPX_3 sulphides calculated within the GGA approximation are 0.44 eV for $CrPS_3$, 1.36 eV for

TABLE III: Total energy relative to the lowest energy magnetic configuration among ferromagnetic (FM), antiferromagnetic (AFM) and non-magnetic (NM) states in single layer transition metal phosphorous trichalcogenide MPX_3. The absence of an entry for a magnetic configuration means that the corresponding state is not metastable. Energies are in meV/unit cell units. Results for for three different exchange-correlation energy functional approximations are compared. Our first principles calculations suggest stable magnetic phases for V, Cr, Mn, Fe, Ni metal compounds. The rectangular and triangular unit cells were shown in Fig. 1. The smaller triangular unit cell is used to compare the NM, FM and Neel AFM phases whereas the larger rectangular unit cell is used when we also compare with the total energies of zAFM, sAFM phases. The work functions are calculated within the GGA are given in eV units.

MPX_3	X	GGA+D2 (Rectangular)					GGA+D2 (Triangular)			GGA (Triangular)			LDA (Triangular)			Work function (eV)		
		NM	FM	AFM	zAFM	sAFM	NM	FM	AFM	NM	FM	AFM	NM	FM	AFM	NM	FM	AFM
	S	1142.8	643.2	0.0	246.9	132.7	1083.8	695.8	0.0	1133.2	665.4	0.0	263.8	276.8	0.0	3.56	3.26	3.42
VPX_3	Se	906.9	275.8	0.0	164.6	87.78	1348.1	458.8	0.0	1389.1	405.6	0.0	503.7	155.1	0.0	2.82	3.57	3.58
	Te						1296.5	183.1	0.0	1237.6	-	0.0	275.3	724.3	0.0	3.08	3.88	3.85
	S	1454.5	0.0	91.65	30.62	63.23	1182.5	0.0	73.68	1220.2	0.0	41.78	275.7	0.0	251.3	3.40	3.07	3.62
$CrPX_3$	Se	1514.6	0.0	146.1	57.06	522.7	1293.7	0.0	315.4	1737.4	0.0	331.7	737.5	0.0	328.6	3.98	3.52	3.65
	Te	1373.4	0.0	242.9	81.31	12.06	1482.6	0.0	264.2	1479.4	0.0	286.2	881.0	0.0	276.9	3.74	3.55	3.41
	S	1576.2	186.3	0.0	60.68	74.59	1964.1	205.4	0.0	2104.9	186.9	0.0	439.7	0.0	352.2	3.74	4.41	3.98
$MnPX_3$	Se	1356.6	156.7	0.0	48.96	68.98	1417.3	166.4	0.0	1351.9	157.7	0.0	510.6	0.0	274.0	3.98	4.07	3.91
	Te	-	-	-	-	-	840.0	12.44	0.0	792.9	17.35	0.0	430.8	0.0	66.08	3.68	3.66	3.77
	S	141.5	286.8	115.8	0.0	289.0	44.87	0.0	308.3	141.1	0.0	329.7	0.0	-	-	3.41	4.13	4.23
$FePX_3$	Se	0.0	-	-	-	-	0.0	165.0	324.5	0.0	162.2	312.2	0.0	-	-	3.93	3.73	3.86
	Te	0.0	-	-	-	-	0.0	-	-	0.0	-	-	0.0	-	-	3.32	-	-
	S	0.0	-	-	-	-	0.0	-	-	0.0	-	-	0.0	-	-	3.84	-	-
$CoPX_3$	Se	0.0	-	-	-	-	0.0	-	-	0.0	-	-	0.0	-	-	4.33	-	-
	Te	0.0	-	-	-	-	0.0	-	-	0.0	-	-	0.0	-	-	3.50	-	-
	S	507.5	276.7	64.16	0.0	343.5	425.1	213.4	0.0	435.8	207.48	0.0	79.55	44.89	0.0	4.63	4.91	5.08
$NiPX_3$	Se	324.8	196.2	0.0	383.2	278.2	168.0	158.8	0.0	166.5	152.5	0.0	0.0	-	-	4.79	4.54	4.44
	Te	0.0	-	-	-	-	0.0	-	-	0.0	-	-	0.0	-	-	2.58	-	-
	S	0.0	-	-	-	-	0.0	-	-	0.0	-	-	0.0	-	-	4.96	-	-
$CuPX_3$	Se	0.0	-	-	-	-	0.0	-	-	0.0	-	-	0.0	-	-	5.15	-	-
	Te	0.0	-	-	-	-	0.0	-	-	0.0	-	-	0.0	-	-	2.96		-
	S	0.0	-	-	-	-	0.0	-	-	0.0	-	-	0.0	-	-	3.97	-	-
$ZnPX_3$	Se	0.0	-	-	-	-	0.0	-	-	0.0	-	-	0.0	-	-	4.47	-	-
	Te	0.0	-	-	-	-	0.0	-	-	0.0	-	-	0.0	-	-	1.11	-	-

$MnPS_3$, 0.24 eV for $FePS_3$, 0.84 eV for $NiPS_3$, 0.01 eV for $CuPS_3$ and 2.19 eV for $ZnPS_3$. These gaps are consistently larger when calculated using the hybrid HSE approximation which includes non-local exchange in the energy functional: 1.61 eV $CrPS_3$, 3.05 eV for $MnPS_3$, 1.83 eV for $FePS_3$, 2.8 eV for $NiPS_3$, 1.76 eV for $CuPS_3$ and 3.11 eV for $ZnPS_3$. A smaller gap enhancement is obtained using a +U interaction correction. (See Table V.) Band gaps are gradually reduced when S is replaced by heavier chalcogen atoms.

The corresponding density of states (DOS) plots are provided in Fig. 5. Again we find that the electron-electron interaction model used in the calculation has an important influence on the electronic structure. The orbital content of the valence and conduction band edges can be extracted from the projected partial density of states (PDOS) results for various MPX_3 compounds presented in Fig. 6. Depending on the specific stoichiometry and on the magnetic configuration of the material under consideration, the valence and conduction band edge orbitals can be dominated by metal, phosphorous or chalcogen atoms. This behavior contrasts from the behavior in the 2D materials classes that have been most extensively studied to date, for example in multilayer graphene systems in which carbon π-bands always dominate or single-layer group-VI transition metal dichalcogenides compounds in which metal d-bands always dominate.

IV. TUNABILITY OF MAGNETIC PROPERTIES

Two dimensional magnetic materials are of interest primarily because of the prospect that their properties might be more effectively altered by tuning parameters that are available *in situ*. Two potentially important control knobs that can be exploited experimentally in two-dimensional-material based nano-devices are carrier-density and strain. The dependence of magnetic properties on carrier density is particularly interesting because it provides a convenient route for electrical manipulation of magnetic properties. In this section we explore the possibility of tailoring the electronic and magnetic properties of MPX_3 ultrathin layers by adjusting carrier density or by subjecting the MPX_3 layers to external strains.

TABLE IV: Magnetic moments in Bohr magneton μ_B units for bulk and single layer MPX_3 structures calculated within GGA+D2, exchange coupling parameters in meV for the three nearest neighbor J_i exchange coupling parameters, and Monte Carlo estimate of the single-layer critical temperatures based on the effective model. The total energy differences are given per MPX_3 formula unit. The magnetization is calculated from the up and down local spin resolved charge density differences as implemented in Quantum Espresso. The critical temperatures estimated are obtained from the peak in the magnetization derivative with respect to temperature as shown in the supplementary information.

MPX_3	X	Bulk		2D							
		FM	AFM	FM	AFM	zAFM	sAFM	J_1	J_2	J_3	T_c
	S	2.03	2.00	1.92	2.01	1.68	1.76	24.5	4.26	3.24	1080
VPX_3	Se	-	-	2.02	2.13	1.77	2.14	10.2	0.340	0.437	770
	Te	-	-	2.22	2.16	2.06	2.19	9.63	-3.59	-7.07	570
	S	2.83	307	2.85	3.14	2.37	2.34	-1.73	-0.015	0.029	281
$CrPX_3$	Se	-	-	2.77	2.83	2.45	2.38	-9.82	-3.49	6.62	1100
	Te	-	-	2.92	2.88	2.82	2.48	-4.89	0.006	-0.087	780
	S	4.24	4.15	4.26	4.16	3.82	3.83	1.21	0.180	0.536	510
$MnPX_3$	Se	-	-	4.25	4.20	4.24	3.82	0.958	0.136	0.506	450
	Te	-	-	4.01	4.11						
	S	3.32	3.14	3.33	3.20	3.24	2.48	-1.59	-0.179	3.00	690
$FePX_3$	Se	-	-	3.28	3.11						
	Te	-	-	0.0	0.0						
	S	0.0	0.0	0.71	0.0						
$CoPX_3$	Se	-	-	0.0	0.0						
	Te	-	-	0.0	0.0						
	S	1.25	1.13	1.26	1.14	1.12	1.20	-11.3	-0.115	36.0	1130
$NiPX_3$	Se	-	-	0.54	0.94	0.12	0.99	127	-82.3	-67.6	2630
	Te	-	-	0.12	0.0						
	S	0.0	0.0	0.0	0.0						
$CuPX_3$	Se	-	-	0.0	0.0						
	Te	-	-	0.0	0.0						
	S	0.0	0.0	0.0	0.0						
$ZnPX_3$	Se	-	-	0.0	0.0						
	Te	-	-	0.0	0.0						

A. Field-effect modification of magnetic properties

The goal of modifying the magnetic properties of a material simply by applying a gate voltage is a holy grail in magnetoelectronics because it could allow magnetically stored information to be written at negligible energy cost. Electric field control of magnetic order has been demonstrated in a number of materials. In ferromagnetic semiconductors the mechanism is carrier density variation in thin films which leads to a modification of the magnetic exchange interaction and magnetic anisotropy. In thin films of ferromagnetic metals, gate voltages can vary the Fermi level position at the interface, which governs the magnetic anisotropy of the metal.[60–62]

We leave to future work a complete microscopic analysis of the response of a MPX_3 layer to a gate voltage when it acts as one electrode of a capacitor. Here we capture the most important response by simply examining the dependence of magnetic properties on carrier density. In doing so we neglect the possible role of charge polarization within a MPX_3 layer. Fig. 7 summarizes the theoretically predicted trends in competition between AFM and FM states in 2D MPX_3 compounds with M = V, Cr, Mn, Fe, Ni metal species and X = S, Se, Te. We find that when the magnetic ground state is AFM (M= V, Mn, Ni, Fe), transitions to FM states are driven by sufficiently large electron or hole carrier densities. The origin of this trend is easy to understand. Because the FM state is gapless the energy changes associated with adding one electron and removing one electron are identical. In the gapped AFM states they differ by the energy gap E_{gap}. It follows that the energy difference per area unit between antiferromagnetic and ferromagnetic states $\delta E \equiv E_{AFM} - E_F$ is given at low carrier densities by

$$\begin{aligned} \delta E(n) &= \delta E_0 + (E_{gap}/2 + \delta\mu)\, n \\ \delta E(p) &= \delta E_0 + (E_{gap}/2 - \delta\mu)\, p \end{aligned} \tag{5}$$

where n is the carrier density of n-type samples, p is the carrier density of p-type samples, δE_0 is the energy difference per area unit between antiferromagnetic and ferromagnetic states in neutral MPX_3 sheets, and $\delta\mu$ is the difference between the mid-gap energy of the antiferromagnetic semiconductors and the chemical potential of the ferromagnetic metals. Introducing n-carriers is most effective in driving a transition from antiferromagnetic to ferromagnetic states when $\delta\mu$ is positive, whereas introducing p-carriers is most effective when $\delta\mu$ is negative. By comparing with Fig. 7 we conclude that $\delta\mu$ is small in most cases, but large and negative in the important cases of the highest critical temperature materials, $MnPS_3$ and

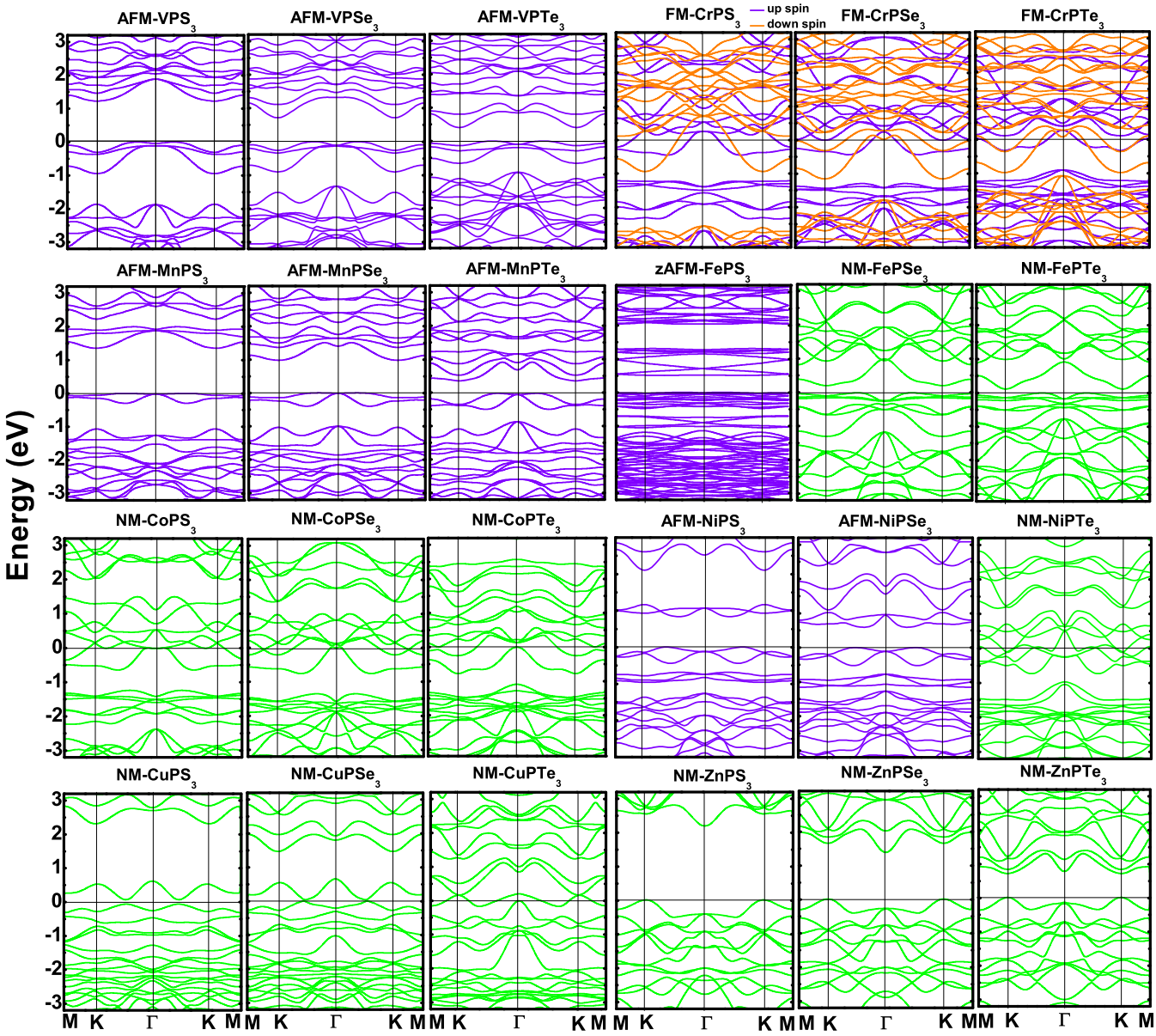

FIG. 4: (Color online) GGA+D2 band structures for single layer MPX_3 compounds in their lowest energy magnetic configuration for M = V, Cr, Mn, Fe, Co, Ni, Cu, and Zn transition metal atoms and X = S, Se, Te chalcogen atoms. The plotted band structures were calculated using the triangular structural unit cell, except for the case of $FePS_3$ which is predicted to have a larger periodicity zAFM (see text) magnetic structure that has a triangular unit cell with a doubled lattice constant. The bands are violet for AFM configurations, violet and orange for the up and down split spin bands in FM configurations, and green NM phases. We note that the AFM phases have semiconducting band gaps and the FM phases are metallic, while the non-magnetic phases can be either metallic or semiconducting. An overall reduction of the band gaps is observed when we use heavier chalcogen atoms, in keeping with the reduction of the covalent bond energy in larger shell orbitals.

$MnPSe_3$. Because the energy difference per formula unit between ferro and antiferromagnetic states is much smaller than the energy gap, a transition between antiferromagnetic and ferromagnetic states can be driven by carrier density changes per formula unit that are much smaller than one - especially so when $\delta\mu$ plays a favorable role. In particular we see in Fig. 7 that a transition between ferromagnetic and antiferromagnetic states are predicted in $MnPS_3$ and $MnPSe_3$ at hole carrier densities that are $\sim 10^{14}\text{cm}^{-2}$ which corresponds to about $\sim$0.16 electrons per formula unit that can be achieved by ionic liquid or gel gating. Transitions between ferromagnetic and antiferromagnetic states are predicted in most materials in most MPX_3 compounds. Our calculations show that the FM solution is the preferred stable magnetic configuration in almost all cases when the system is subject to large electron or hole densities in the range above a few times $\pm 10^{14}$

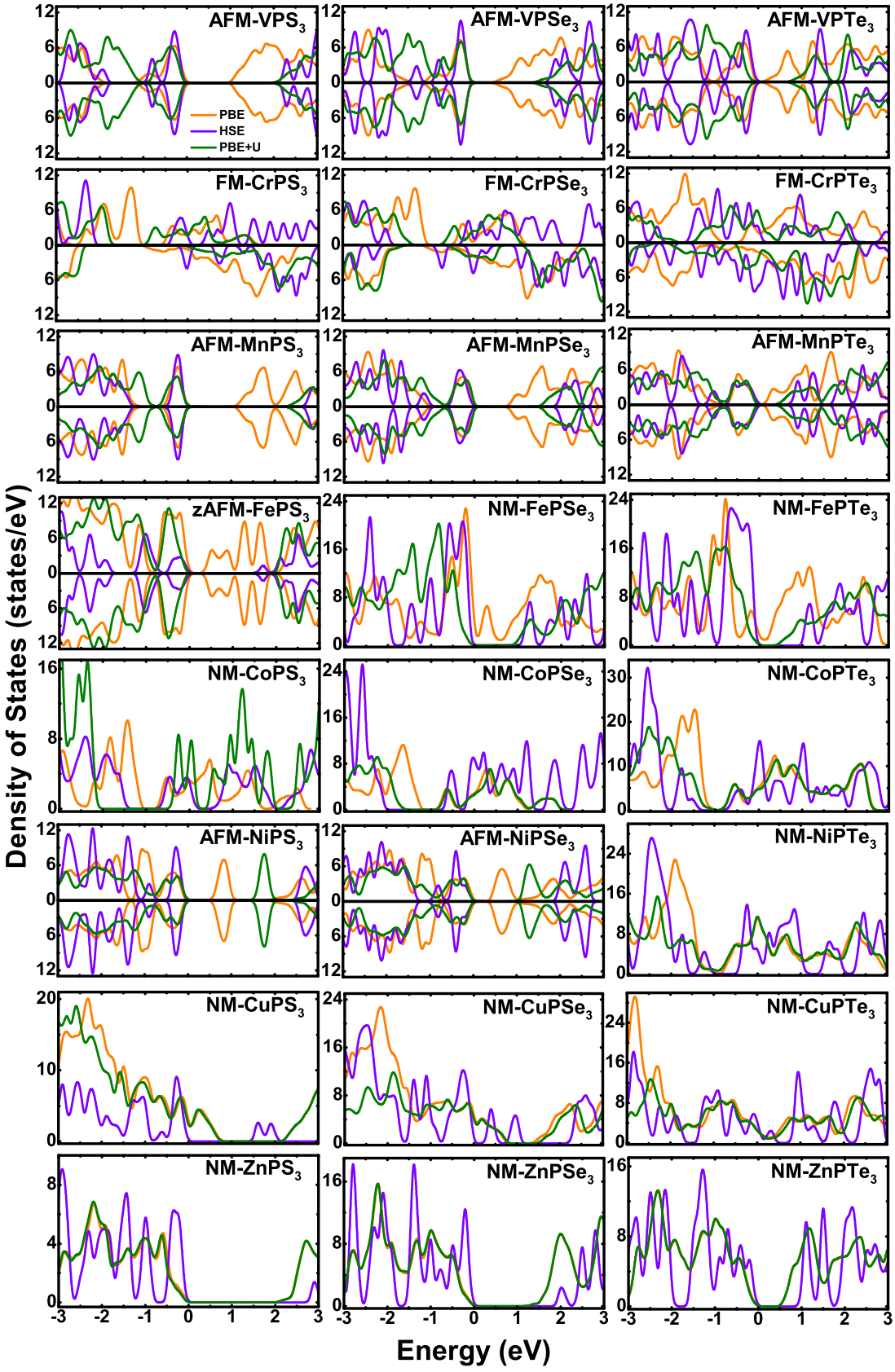

FIG. 5: (Color online) Total density of states (DOS) for the magnetic ground-states in Fig. 4, calculated using three different exchange-correlation energy functional calculations GGA, HSE and GGA+U. We have placed the valence band edge at $E = 0$. Overall band gap enhancements are found for the semiconducting phases when additional electron-electron interactions are approximated as a non-local exchange corrections in HSE and as onsite repulsion corrections in GGA+U. Both HSE and GGA+U enhance the band gap magnitudes . Other features in the DOS plots also depend on the DFT exchange-correlation functional approximation.

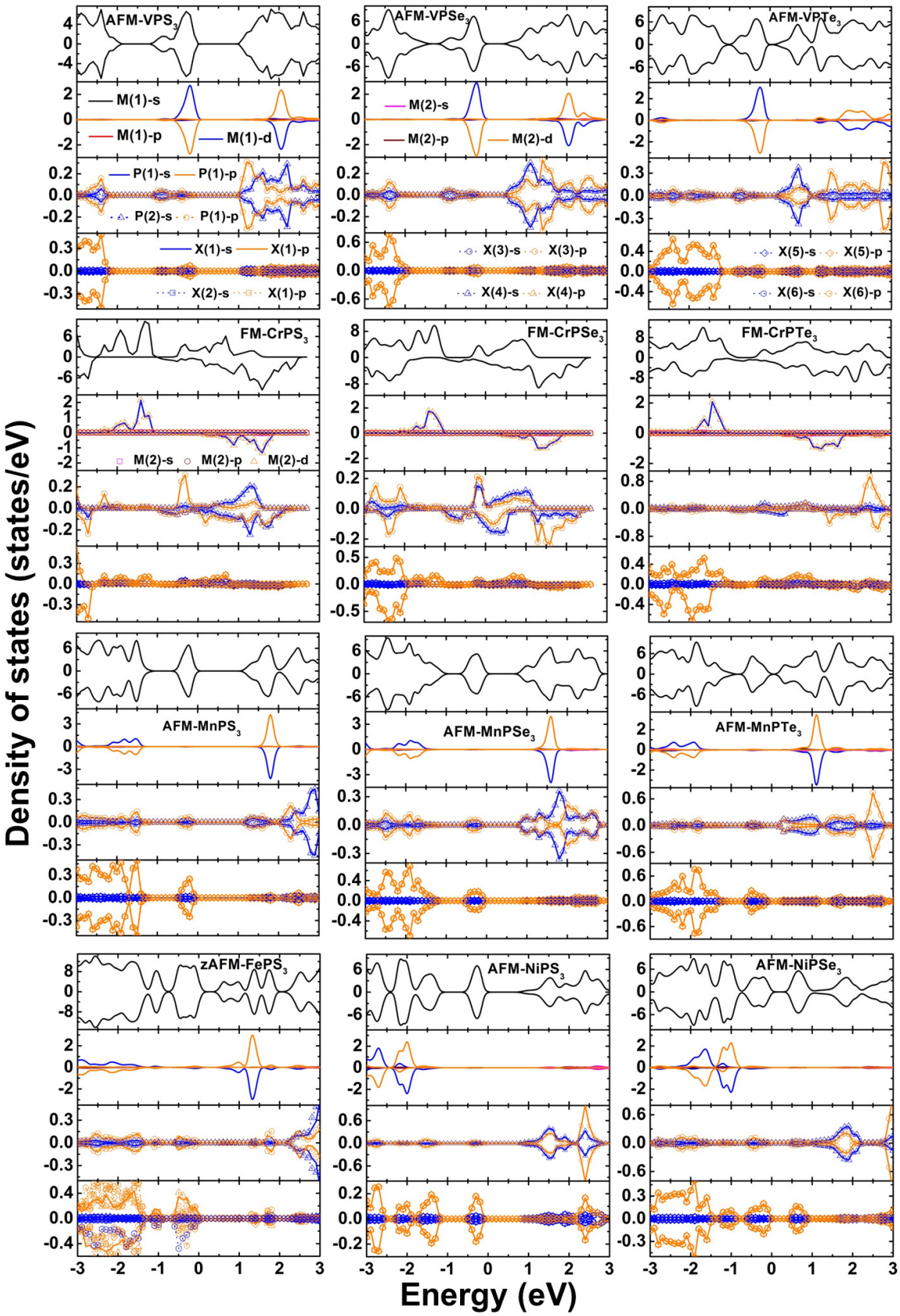

FIG. 6: (Color online) Orbital projected partial density of states (PDOS) calculated for self-consistently converged ground-state magnetic configurations. The valence band edge located at $E = 0$. From the PDOS of the various MPX_3 compounds we observe that the orbital content of the valence and conduction band edges do not generally consist of the same atomic orbital contributions and vary widely depending on the specific choice for each one of the atoms constituting the material and the magnetic configuration. For the compounds showing carrier-dependent tunability of the magnetic phases the states closest to the Fermi energy have generally an important contribution from the p-orbitals of the chalcogen and P atoms.

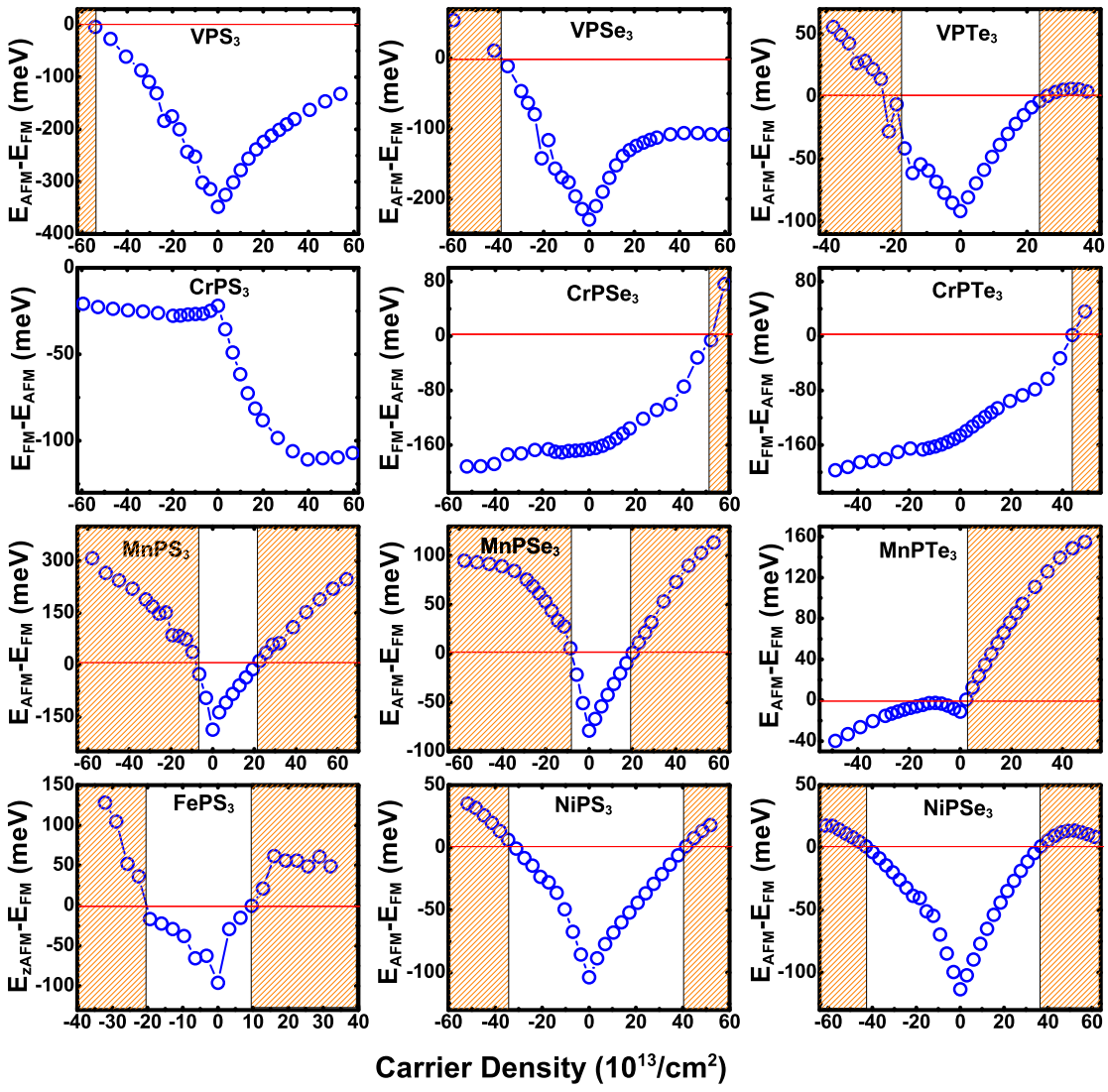

FIG. 7: (Color online) Carrier density dependent total energy differences per MPX_3 formula unit between the AFM and FM states of V, Cr, Mn, Fe, Ni based single layer trichalcogenides. The prominent cusps in these curves appear because the the antiferromamgnetic state has a band gap whereas the ferromagnetic state does not have a band gap. The AFM ground-states favored near charge neutrality can be switched to FM states at accessible carrier densities in V, Mn, Ni, and Fe based compounds. For $CrPX_3$ with X = Se or Te, it is possible to switch from a FM to an AFM state at finite n-doping. Carrier densities of up to a few $\sim 10^{14}$ electrons per cm^2 should be in principle accessible through ionic liquid or gel gating. The carrier density of 0.1 electrons per MPX_3 formula unit corresponds to $\sim 6 \times 10^{13}$ electrons per cm^2 when the lattice constant is $\sim 6\AA$.

cm^{-2}. In 2D materials these large carrier densities are, in principle, achievable using ionic liquid or gel gating techniques. Our calculations motivate efforts to find materials which can be used to establish good electrical contacts to MPX_3 compounds, and in particular to the valence bands of $MnPS_3$ and $MnPSe_3$. These results establish that the magnetic properties of $MnPX_3$ two-dimensional materials are sensitive to carrier density. For the Cr based compound, whose behavior is different to other compounds within this class of materials, the ground states at zero carrier density is FM and we find that a transition to an AFM state occurs for *n*-doped systems.

B. Strain-tunable magnetic properties

The membrane-like flexibility of ultrathin 2D materials makes them suitable platforms for tailoring the electronic structure properties by means of strains. Representative examples on effects of strains in 2D materials properties that have been discussed in recent literature include the observation of Landau-level like density of states near high curvature graphene bubbles[63], or the commensuration moire strains that opens up a band gap at the primary Dirac point in graphene on hexagonal boron nitride for sufficiently long

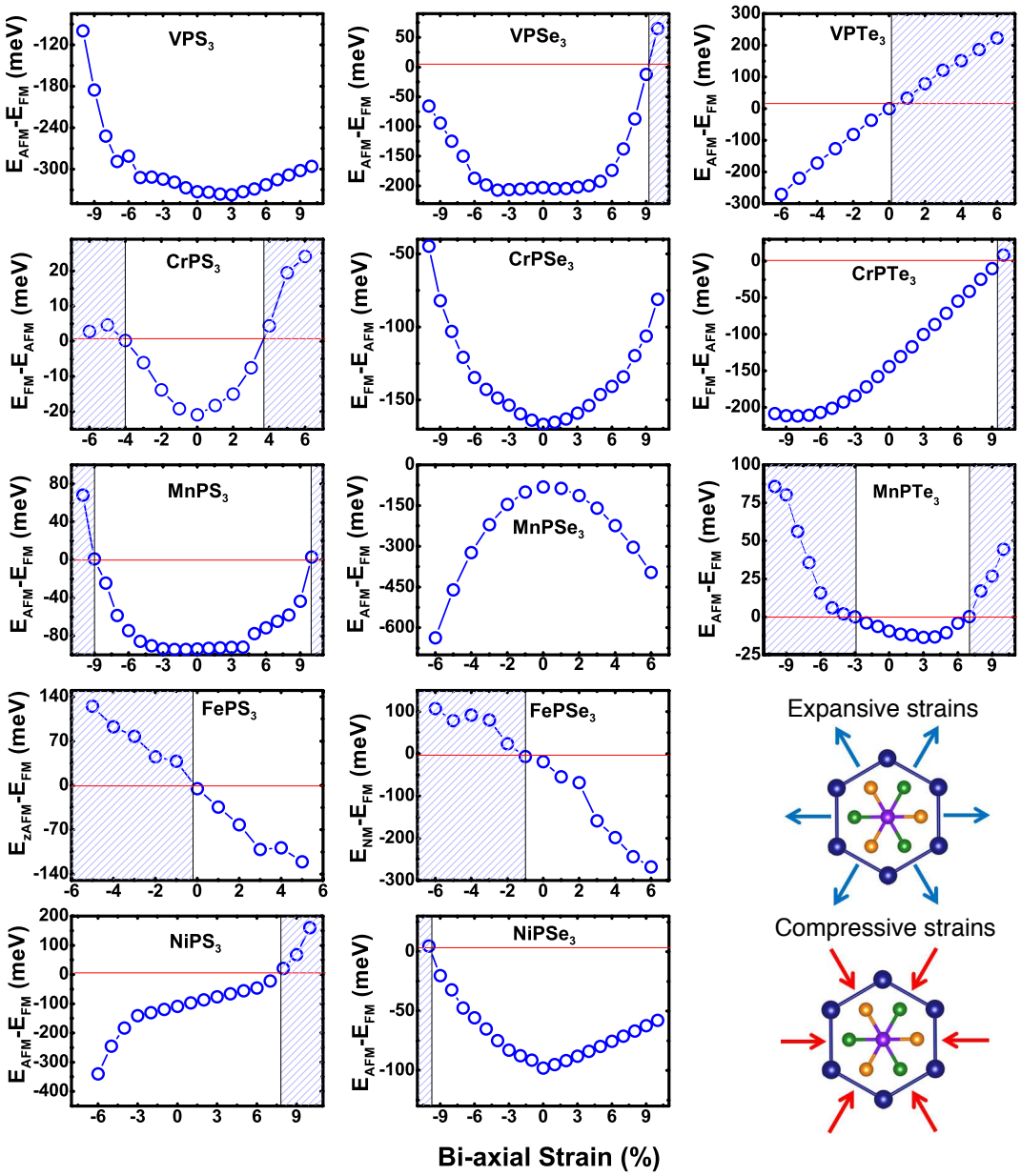

FIG. 8: (Color online) Influence of in-plane strain on the magnetic configurations of different MPX_3 compounds. Magnetic phase transition introduced by in-plane biaxial compressive and expansive strains for several magnetic MPX_3 compounds at neutral carrier densities. Particularly sensitive strain dependence is seen for $FePS_3$, $FePSe_3$ and $VPTe_3$ where small strains on the order of 1% of the lattice constant can switch the magnetic phases.

moire patterns[64–66]. The sensitive variation of the different M-M, P-P, M-X bond lengths as a function of magnetic configuration we have presented earlier in Sec. III suggests that strains can be used as switches to trigger magnetic phase transitions or alter the stability of the magnetic phases by modifying the total energy difference with respect to the non-magnetic phases. Here we have carried out calculations of the total energies for different magnetic phases to explore the influence of expansive or compressive in-plane biaxial and uniaxial strains and the effects of external pressure along the out-of plane axis in 2D MPX_3 materials. The compressive and expansive biaxial strains have been modeled through uniform scaling of the rectangular unit cell in Fig. 1 and likewise the uniaxial strains are modeled by scaling the unit cell either in the zigzag or armchair directions. We notice that generally the effects of uniform biaxial versus uniaxial strains introduce modifications in the magnetic phase energy difference total energies that are qualitatively similar for the compressive or expansive strains, and that the effects are stronger for biaxial strains when compared to unixaxial strains which do not show

TABLE V: Band gaps of MPX_3 compounds predicted to have antiferromagnetic semiconductor ground states. The band gaps are listed in eV energy units and have values that depend substantially on the DFT exchange-correlation approximation employed. Values are listed for GGA+D2, HSE hybrid functional and GGA+U approximations. The magnitude of U was chosen to to maximize the band gap. As expected the HSE functional yields the largest band gaps.

	X	GGA+D2	HSE	GGA+U
	S	1.23	2.50	2.32 (U = 3.25)
VPX_3	Se	0.73	2.10	1.67 (U = 3.25)
	Te	0.41	1.57	1.00 (U = 3.25)
	S	1.36	3.05	2.34 (U = 5.0)
$MnPX_3$	Se	0.98	2.24	1.70 (U = 5.0)
	Te	0.38	1.06	0.69 (U = 5.0)
	S	0.57	2.07	2.26 (U = 5.3)
$FePX_3$	Se	0.20	1.48	1.19 (U = 5.3)
	Te	0.13	1.35	0.59 (U = 5.3)
	S	0.84	2.83	1.74 (U = 6.45)
$NiPX_3$	Se	0.59	2.22	1.31 (U = 6.45)
	Te	-	0.27	-
	S	0.01	1.76	0.08 (U = 1.0)
$CuPX_3$	Se	-	0.56	-
	S	2.19	3.11	2.23 (U = 5.4)
$ZnPX_3$	Se	1.38	2.19	1.41 (U = 5.4)
	Te	0.73	1.26	0.74 (U = 5.4)

a noticeable difference between the zigzag or armchair directions. Pressure strains along the out of plane vertical c-axis have been applied by artificially modifying the P-P distance and we find for $MnPS_3$ a clear transition from AFM to FM with the total energy difference $E_{\rm AFM} - E_{\rm FM}$ changing from -93 meV to 268 meV per formula unit in the presence of a -4% bond length shortening strain for the P-P distance. Relatively large strains are required to alter the magnetic properties in compounds like $MnPS_3$ but other systems such as $CrPS_3$, $FePS_3$, $FePSe_3$ $NiPS_3$ and $VPTe_3$ the magnetic phase transitions can be achieved for smaller strains as they have relatively smaller total energy differences between the magnetic phases. We find a particularly sensitive transition near charge neutrality for $FePS_3$, $FePSe_3$ and $VPTe_3$ where strains on the order of $\sim$1% is enough to switch between different magnetic configurations.

V. SUMMARY AND DISCUSSIONS

In this paper we have carried an *ab initio* study of MPX_3 transition metal phosphorous trichalcogenide for different combinations of 3d metals (M = Cr, Mn, Fe, Co, Ni, Cu, Zn) and chalcogens (X = S, Se, Te) in search for candidate materials that can exhibit intrinsic magnetism in the 2D single layer limit. Our calculations suggest that magnetic phase is intrinsic for each individual layer of van der Waals materials and various magnetic phases are expected in single layer MPX_3 phosphorous trichalcogenides depending on the various combinations of transition metals and chalcogen atoms.

The calculations suggest that the semiconducting Néel antiferromagnetic phases are the most common form of magnetic configuration (we find AFM phase for V, Mn, Fe, Ni based compounds). A metallic ferromagnetic phase is found in Cr based compounds, while the non-magnetic phases are found in either semiconducting or metallic electronic structure. As expected from the weaker covalent bond energy in larger atomic orbitals, we find that for the semiconducting antiferromagnetic materials the replacing a smaller chalcogen atom with larger chalcogen atoms induces a smaller band gap energy, as a consequence the difference of the ground state energies between FM and AFM phases becomes smaller. A further interesting analysis in future work is the magnetic properties of $CoPX_3$ in which we do not find a magnetic phase in spite of a typically magnetic atom. We find that the electronic structure and band gap is rather sensitive to the choice of the exchange-correlation energy functional and the model for the Coulomb interaction, as manifested in the large discrepancies in the density of states between the standard semilocal GGA, local onsite U corrected calculations or the hybrid functionals with non-local exchange. This sensitivity of the optimized ground-state results to the choice of the approximation scheme makes it desirable to benchmark the results against experiments in order to establish reliable theoretical models to further our study.

An interesting interdependence between magnetic order and atomic structure was found with typical variations on the order of a few percents in the lattice constant and interatomic bond lengths leading to structural distortions depending on the magnetic configuration of the system. The bond length variations were traced through M-M, P-P, P-X bond distances associated with the distortions in the honeycomb array of the transition metal atoms and the distance between the atomic centers in the $(P_2X_6)^{4-}$ bipyramids. We leave for future work the analysis on the role of spin-orbit coupling effects and optical properties arising from lattice symmetry breaking coupled to the onset of magnetism. Sizable differences between the GGA and the LDA solutions is suggestive of the delicate balance between the different chemical bonds for configuring the optimized structure of these compounds which in turn are affected by the onset of magnetism.

In 2D MPX_3 different stable and meta-stable magnetic configurations were found. The semiconducting states with a band gap are typically antiferromagnetic phases in either Néel, zigzag, or stripy configuration and the metallic states are typically ferromagnetic phases. The critical temperatures for the magnetic phases in the single layer limit is expected in principle to be smaller than the bulk due to the absence of interlayer exchange that can further stabilize the magnetic phase. We analyzed the magnetic phases of the 2D MPX_3 by building an effective model Hamiltonian with the exchange coupling parameters extracted by mapping the total energies from our *ab initio* calculations onto an effective model. The Curie and Néel temperatures T_C, T_N are obtained by using a statistical analysis based on the Metropolis algorithm[58]. The calculated Néel temperatures of the antiferrmomagnetic compounds with the effective model Hamiltonian has a wide range of variation

ranging between a few to a few hundred Kelvins depending on the composition.

The control of the magnetic phases with electric field in field effect transistor devices is particularly appealing for magnetic 2D material based devices where the carrier density in the devices can be controlled through appropriate gating. Our calculations indicate that the transition between antiferromagnetic to ferromagnetic phases can be achieved by inducing carrier densities in the 2D MPX_3 as low as 10^{13} cm^{-2} to values as large as $10^{15} cm^{-2}$ whose range can partially be covered in the field effect transistor devices using a backgate. The actual feasibility and device performance for inducing carrier densities depends sensitively on the specific electronic structure of the material under consideration. In 2D MPX_3 the gating effect is easier for metals and becomes more limited for semiconductors. We find that the tuning of carrier density in the metallic $CrPSe_3$ and $CrPTe_3$ compounds is most promising because the magnetic phase transition from FM to AFM phases is observed for electron densities on the order of $5 \cdot 10^{13}$ cm^{-2}. Also, the AFM to FM transitions in $VPTe_3$, $MnPTe_3$, and $FePS_3$ can be easily achieved by electric gating because they have relatively small GGA band gaps on the order of $\sim$0.5 eV. For materials exhibiting magnetic phases we find that using larger chalcogen Te can reduce the carrier densities required for the magnetic transition. Somewhat larger carrier densities of a few tens of 10^{13} cm^{-2} is needed for Mn, Ni based sulphides and selenides. For the materials with a large band gap of the order of eVs the switching of magnetic phases is also possible with the use of higher dielectric constant materials or ferroelectric polymers which could allow reaching large enough carrier densities. The use of larger chalcogen atoms or forming appropriate heterogeneous mix of transition metal atoms reduces the semiconducting band gap size in AFM phases.

The interdependence between atomic and electronic structure allows to make use of strains to tune the energetically favored magnetic phase. We have found that the ground state magnetic configuration can undergo phase transitions in the presence of in-plane compression and expansion of the lattice constants, as well as c-axis pressure. The magnitude of the required strains vary greatly, with values below 1% for compounds such as $FePS_3$, $FePSe_3$ and $VPTe_3$, and larger strains on the order of or far greater than 4% are required to trigger a FM-AFM magnetic phase transition in $CrPS_3$ and $NiPS_3$. Phase transitions for even larger strains on the order of $\sim$9% are observed in $VPSe_3$, $MnPS_3$, $NiPS_3$, $NiPSe_3$ whose non-strained configuration has a robust gapped antiferromagnetic phase.

In conclusion, we propose the single layer of different MPX_3 transition metal thiophosphate as candidate materials with intrinsic 2D magnetic properties. The MPX_3s are in principle tunable through the application of external strains or by modifying the carrier densities in field effect transistor devices. In addition, the transition temperatures can be controlled through external gate voltage and strains. The sensitivity of these systems to variations in the system parameters, such as composition stoichiometry, details of the interface, and the exchange coupling of the magnetic properties with external fields, offers ample room for future research that seek new functionalities. From our theoretical work we have been able to draw some general conclusions on the property trends of MPX_3 materials as a function of composition, and their expected electronic and magnetic properties. Because of the inherent uncertainties in currently available *ab initio* calculation methods it is desirable to accompany theoretical modelization using input data from experiments for the feasibility study of their practical implementation in spintronic devices.

VI. ACKNOWLEDGEMENTS

We are thankful to the assistance and computational resources from Texas Advanced Computing Centre (TACC). This work has been supported by the 2015 Research Fund of the University of Seoul for JJ. Also, this work was supported by NRF-2014R1A2A2A01006776 for EHH, ONR-N00014-14-0330 and Welch Foundation grant TBF1473 for AHM, and NRF-2015R1D1A1A01060381 for MH. We acknowledge helpful discussions with J. D. Noh on the calculation of the critical temperatures of the magnetic phases.

* Electronic address: heh8232@gmail.com
† Electronic address: jeil.jung@gmail.com

[1] K. S. Novoselov, A. K. Geim, S. V. Morozov, D. Jiang, M. I. Katsnelson, I. V. Grigorieva, S. V. Dubonos and, A. A. Firsov, Two-dimensional gas of massless Dirac fermions in graphene, Nature **438**, 197 (2005).
[2] Y. Zhang, Y.-W. Tan, H. L. Stormer, and P. Kim, Experimental observation of the quantum Hall effect and Berry's phase in graphene, Nature **438**, 201 (2005).
[3] K. S. Novoselov, D. Jiang, F. Schedin, T. J. Booth, V. V. Khotkevich, S. V. Morozov, and A. K. Geim, Two-dimensional atomic crystals, Proc. Nat. Ac. Sci. **102**, 10451 (2004).
[4] M. Chhowalla, H. S. Shin, G. Eda, L-J. Li, K. P. Loh and, H. Zhang, The chemistry of two-dimensional layered transition metal dichalcogenide nanosheets, Nature Chemistry **5**, 263 (2013).
[5] L. Britnell, R. M. Ribeiro, A. Eckmann , R. Jalil, B. D. Belle, A. Mishchenko, Y. J. Kim, R. V. Gorbachev, T. Georgiou, S. V. Morozov, A. N. Grigorenko, A. K. Geim, C. Casiraghi, A. H. Castro Neto, K. S. Novoselov KS, Strong light-matter interactions in heterostructures of atomically thin films, Science 340, 1311 (2013).
[6] B. Burk, R. E. Thomson, J. Clarke, A. Zettl, Surface and Bulk Charge Density Wave Structure in 1 T-TaS2, Science 257, 362 (1992).
[7] A. H. Castro Neto, Charge Density Wave, Superconductivity, and Anomalous Metallic Behavior in 2D Transition Metal Dichalcogenides, Phys. Rev. Lett. **86**, 4382 (2001).
[8] R. F. Frindt, Superconductivity in ultrathin NbSe2 layers, Phys. Rev. Lett. 28, 299 (1972).

[9] D. Costanzo, S. Jo, H. Berger, and A. F. Morpurgo, Gate-induced superconductivity in atomically thin MoS_2 crystals, Nature Nanotechnology, doi:10.1038/nnano.2015.314 (2016).

[10] L. J. de Jongh, Magnetic Properties of Layered Transition Metal Compounds Volume 9 of the series Physics and Chemistry of Materials with Low-Dimensional Structures.

[11] Y. Ma, Y. Dai, M. Guo, C. Niu, Y. Zhu, and B. Huang, Evidence of the Existence of Magnetism in Pristine VX_2 Monolayers (X = S, Se) and Their Strain-Induced Tunable Magnetic Properties, ACS Nano, **6**, 1695 (2012).

[12] S. Lebegue, T. Björkman, M. Klintenberg, R. M. Nieminen, and O. Eriksson, Two-Dimensional Materials from Data Filtering and Ab Initio Calculations, Phys. Rev. X **3**, 031002 (2013).

[13] B. Siberchicot, S. Jobic , V. Carteaux , P. Gressier , and G. Ouvrard, Band Structure Calculations of Ferromagnetic Chromium Tellurides CrSiTe3 and CrGeTe3, J. Phys. Chem. **100**, 5863, (1996).

[14] Strong spin-lattice coupling in $CrSiTe_3$, L. D. Casto, A. J. Clune, M. O. Yokosuk, J. L. Musfeldt, T. J. Williams, H. L. Zhuang, M.-W. Lin, K. Xiao, R. G. Hennig, B. C. Sales, J.-Q. Yan, and D. Mandrus, APL Mater. 3, 041515 (2015).

[15] T. J. Williams, A. A. Aczel, M. D. Lumsden, S. E. Nagler, M. B. Stone, J.-Q. Yan, D. Mandrus, Magnetic Correlations in the Quasi-2D Semiconducting Ferromagnet $CrSiTe_3$, Phys. Rev. B 92, 144404 (2015).

[16] H. L. Zhuang, Y. Xie, P. R. C. Kent, and P. Ganesh, Computational discovery of ferromagnetic semiconducting single-layer CrSnTe3, Phys. Rev. B 92, 035407 (2015).

[17] X. Chen, J. Qi, and D. Shi, Strain-engineering of magnetic coupling in two-dimensional magnetic semiconductor CrSiTe3: Competition of direct exchange interaction and superexchange interaction, Physics Letters A, **379**, 60 (2015).

[18] M.-W. Lin, H. L. Zhuang, J. Yan, T. Z. Ward, A. A. Puretzky, C. M. Rouleau, Z. Gai, L. Liang, V. Meunier, B. G. Sumpter, P. Ganesh, P. R. C. Kent, D. B. Geohegan, D. G. Mandrus and K. Xiao, Ultrathin nanosheets of CrSiTe3: a semiconducting two-dimensional ferromagnetic material J. Mater. Chem. C, **4**, 315 (2016).

[19] N. Sivadas, M. W. Daniels, R. H. Swendsen, S. Okamoto, and D. Xiao, Magnetic ground state of semiconducting transition-metal trichalcogenide monolayers, Phys. Rev. B. **91**, 235425 (2015).

[20] M. A. McGuire, H. Dixit, V. R. Cooper, and B. C. Sales, Coupling of Crystal Structure and Magnetism in the Layered, Ferromagnetic Insulator CrI_3, Chem. Mater., **27**, 612 (2015).

[21] W. B. Zhang, Q. Qu, P. Zhu, C. H. Lam, Robust intrinsic ferromagnetism and half semiconductivity in stable two-dimensional single-layer chromium trihalides, J. Mater. Chem. C, **3**, 12457 (2015).

[22] X. Li, T. Cao, Q. Niu, J. Shi, and J. Feng, Coupling the valley degree of freedom to antiferromagnetic order, Proc. Nat. Ac. Sci. **110**, 3738 (2013).

[23] X. Li, X. Wu, and J. Yang, Half-Metallicity in $MnPSe_3$ Exfoliated Nanosheet with Carrier Doping, J. Am. Chem. Soc. **136**, 11065 (2014).

[24] R. Brec, Review on structural and chemical properties of transition metal phosphorous trisulfides MPS_3, Solid State Ionics **22**, 3, (1986).

[25] E. Prouzet, G. Ouvrard and R. Brec, Structure determination of $ZnPS_3$, Mat. Res. Bull., **21**, 195, (1986).

[26] G. Ouvrard, R. Brec and J. Rouxel, Structural determination of some MPS_3 layered phases (M = Mn, Fe, Co, Ni and Cd), Mat. Res. Bull., **20**, 1181, (1985).

[27] G. Ouvrard, R. Freour, R. Brec and J. Rouxel, A mixed valence compound in the two dimensional MPS_3 family: $V_{0.78}PS_3$ structure and physical properties, Mat. Res. Bull., **20**, 1053, (1985).

[28] P. A. Joy and S. Vasudevan, Infrared(700-100 cm^{-1}) vibrational spectra of the layered transition metal thiophosphates, MPS_3, (M = Mn, Fe AND Ni), J. Phys. Chem. Solids **54**, 343, (1993).

[29] K. C. Rule, Magnetic ordering in the two dimensional antiferromagnet $FePS_3$, Doctoral Thesis, School of Physics and Material Engineering, Monash University, Australia, (2004).

[30] E. Ressouche, M. Loire, V. Simonet, R. Ballou, A. Stunault, and A. Wildes Magnetoelectric $MnPS_3$ as a candidate for ferrotoroidicity, Phys. Rev. B **82**, 100408(R) (2010).

[31] K. Kurosawa, S. Saito, and Y. Yamaguchi,Neutron Diffraction Study on $MnPS_3$ and $FePS_3$, J. Phys. Soc. Jpn. **52**, 3919 (1983).

[32] W. Klingen, G. Eulenberger, and H. Hahn, Implementation of nitrogen trifluoride with methyl and thylmagnesiumbromid, Nature of Sciences. **55**, 229 (1968).

[33] N. Kurita and K. Nakao, Band structure of magnetic layered semiconductor NiPS3, J. Phys. Soc. Jpn. **58**, 232 (1989).

[34] K. C. Rule, G. J. McIntyre, S. J. Kennedy, and T. J. Hicks, Single-crystal and powder neutron diffraction experiments on $FePS_3$: Search for the magnetic structure Phys. Rev. B **76**, 134402, (2007).

[35] N. Kurita and K. Nakao, Band Structures and Physical Properties of Magnetic Layered Semiconductors MPS_3, J. Phys. Soc. Jpn. **58**, 610 (1989).

[36] G. Le Flem, R. Brec, G. Ouvard, and A. Louisy, P. Segransan, Magnetic interactions in the layer compunds MPX_3 (M=Mn,Fe,Ni;X=S,Se) J. Phys. Chem. Solids, **43**, 455, (1982).

[37] D. J. Goossens, Dipolar anisotropy in quasi-2D honeycomb antiferromagnet $MnPS_3$, Eur. Phys. J. B **78**, 305 (2010).

[38] N. Chandrasekharan and S. Vasudevan, Magnetism, exchange and crystal field parameters in the orbitally unquenchedlsing antiferromagnet $FePS_3$, Pramana Journal of Physics, **43**, 21, (1994).

[39] P. Jeevanandam and S. Vasudevan, Magnetism in MnPSe3: a layered $3d^5$ antiferromagnet with unusually large XY anisotropy, J. Phys.: Condens. Matter 11 (1999) 3563?3570.

[40] P. A. Joy and S. Vasudevan, Magnetism in the layered transition-metal thiophosphates MPS_3 (M =Mn, Fe, and Ni), Phys. Rev. B, 46, 5425 (1992).

[41] A R Wildes, K C Rule, R I Bewley, M Enderle and T J Hicks, The magnon dynamics and spin exchange parameters of $FePS_3$, J. Phys.: Condens. Matter **24**, 416004 (2012).

[42] A R Wildes. S J Kennedy and T J Hicks, True two-dimensionalmagnetic ordering in $MnPS_3$, J. Phys.: Condens. Matter **6**, 335 (1994).

[43] J. Liu, X.-B. Li, D. Wang, W.-M. Lau, P. Peng, and L.-M. Liu, Diverse and tunable electronic structures of single-layer metal phosphorus trichalcogenides for photocatalytic water splitting, The Journal of Chemical Physics **140**, 054707 (2014).

[44] K.Z. Du, X.Z. Wang, Y. Liu, P. Hu, M.I.B. Utama, C.K. Gan, Q.H. Xiong, and C. Kloc, Weak Van der Waals Stacking, Wide-Range Band Gap, and Raman Study on Ultrathin Layers of Metal Phosphorus Trichalcogenides, ACS Nano 10(2), 1738-1743 (2016).

[45] R. Brec, D.M. Schleigh, G. Ouvrard, A. Louisy, and J. Rouxel, Physical Properties of Lithium Intercalation Compounds of the Layered Transition Chalcogenophosphates, Inorganic Chemistry, Vol. **18**, 1814 (1979).

[46] P. J. S. Foot, T. Katz, S. N. Patel, B. A. Nevett, A. R. Piercy, and A. A. Balchin, The structures and conduction mechanisms of lithium-intercalated and lithium-substituted nickel phosphorus trisulphide ($NiPS_3$), and the use of the material as a secondary battery electrode, Phys. Status Solidi A **100**, 11 (1987).

[47] P. J. S. Foot and B. A. Nevett, Electronic Conduction in p- and n-Type $NiPS_3$, Phys. Stat. Sol. A **93**, 283 (1986).

[48] R. Clement, Ion-Exchange Intercalation into the MPS_3 Layered

Compounds Hybrid Organic-Inorganic Composites, Edited by:J. E. Mark, C. Y-C Lee, P. A. Bianconi, ACS Symposium Series, **585**, 29 (1995).

[49] R. Clement, J. P. Audiere, O. Poizat, and C. Sourisseau, Y. Mathey, Structural, vibrational and conduction properties of a new class of layer-type MPS_3 compounds, Mn^{II}_{1-x} $M^{I}_{2x}PS_3$ (M^I = Cu, Ag), Solid state ionics 9&10, 459 (1983).

[50] P. Giannozzi, S. Baroni, N. Bonini, M. Calandra, R. Car, C. Cavazzoni, D. Ceresoli, G. L. Chiarotti, M. Cococcioni, I. Dabo, A. D. Corso, S. de Gironcoli, S. Fabris, G. Fratesi, R. Gebauer, U. Gerstmann, C. Gougoussis, A. Kokalj, M. Lazzeri, L. Martin-Samos, N. Marzari, F. Mauri, R. Mazzarello, S. Paolini, A. Pasquarello, L. Paulatto, C. Sbraccia, S. Scandolo, G. Sclauzero, A. P. Seitsonen, A. Smogunov, P. Umari, and R. M. Wentzcovitch, QUANTUM ESPRESSO: a modular and open-source software project for quantum simulations of materials, J. Phys.: Cond. Matter **21**, 395502 (2009).

[51] J. P. Perdew, K. Burke, and M. Ernzerhof, Generalized Gradient Approximation Made Simple, Phys. Rev. Lett. **77**, 3865 (1997).

[52] S. Grimme, Semiempirical GGA-type density functional constructed with a long-range dispersion correction, J. Comp. Chem. **27**, 1787 (2006).

[53] J. P. Perdew and A. Zunger, Self-interaction correction to density-functional approximations for many-electron systems, Phys. Rev. B 23, 5048 (1981).

[54] N. Marom, J. Bernstein, J Garel, A. Tkatchenko, E. Joselevich, L. Kronik, and O. Hod, Stacking and Registry Effects in Layered Materials: The Case of Hexagonal Boron Nitride, Phys. Rev. Lett. **105**, 046801 (2010).

[55] J. Heyd, G. Scuseria, and M. Ernzerhof, Hybrid functionals based on a screened Coulomb potential, J. Chem. Phys., **118**, 8207 (2003).

[56] J. Chaloupka, G. Jackeli, and G. Khaliullin, Zigzag Magnetic Order in the Iridium Oxide Na_2IrO_3, Phys. Rev. Lett. **110**, 097204 (2013).

[57] N. Sivadas, M. W. Daniels, R. H. Swendsen, S. Okamoto, and D. Xiao, Phys. Rev. B 91, 235425 (2015).

[58] N. Metropolis, A. W. Rosenbluth, M. N. Rosenbluth, A. H. Teller, E. Teller, J. Chem. Phys. 21, 1087 (1953).

[59] D. P. Landau, S.-H. Tsai, and M. Exler, A new approach to Monte Carlo simulations in statistical physics: Wang-Landau sampling, Am. J. Phys. **72**, 10 (2004).

[60] F. Matsukura, Y. Tokura, and Hideo Ohno, Control of magnetism by electric fields, Nature Nanotechnology 10, 209 (2015).

[61] H. Ohno, D. Chiba, F. Matsukura, T. Omiya, E. Abe, T. Dietl, Y. Ohno, and K. Ohtani, Electric-field control of ferromagnetism, Nature 408, 944 (2000).

[62] M. Endo, S. Kanai, S. Ikeda, F. Matsukura and H. Ohno, Electric-field effects on thickness dependent magnetic anisotropy of sputtered $MgO/Co_{40}Fe_{40}B_{20}$/Ta structures, App. Phys. Lett. 96, 212503 (2010).

[63] N. Levy, S. A. Burke, K. L. Meaker, M. Panlasigui, A. Zettl, F. Guinea, A. H. Castro Neto, M. F. Crommie, Strain-Induced Pseudo-Magnetic Fields Greater Than 300 Tesla in Graphene Nanobubbles, Science 329, 544 (2010).

[64] B. Hunt, J. D. Sanchez-Yamagishi, A. F. Young, M. Yankowitz, B. J. LeRoy, K. Watanabe, T. Taniguchi, P. Moon, M. Koshino, P. Jarillo-Herrero, and R. C. Ashoori, Massive Dirac Fermions and Hofstadter Butterfly in a van der Waals Heterostructure, Science 340, 1427 (2013).

[65] C. R. Woods, L. Britnell, A. Eckmann, R. S. Ma, J. C. Lu, H. M. Guo, X. Lin, G. L. Yu, Y. Cao, R. V. Gorbachev, A. V. Kretinin, J. Park, L. A. Ponomarenko, M. I. Katsnelson, Yu. N. Gornostyrev, K. Watanabe, T. Taniguchi, C. Casiraghi, H-J. Gao, A. K. Geim and K. S. Novoselov, Commensurate-incommensurate transition in graphene on hexagonal boron nitride, Nat. Phys. **10**, 451 (2014).

[66] J. Jung, A. M. DaSilva, A. H. MacDonald, and Shaffique Adam, Origin of band gaps in graphene on hexagonal boron nitride, Nat. Commun. 6:6308 doi: 10.1038/ncomms7308 (2015).